inorganics

MDPI

Article

Synthesis, Characterization, and Impact of Water on the Stability of Postmodified Schiff Base Containing Metal–Organic Frameworks

Nikola D. Radnović [1,*], Chris S. Hawes [2], Branko B. Kordić [1], Milica G. Bogdanović [1], Berta Barta Holló [1], Mirjana M. Radanović [1], Dušan Đ. Škorić [1], Branislav D. Jović [1] and Marko V. Rodić [1,*]

[1] Faculty of Sciences, University of Novi Sad, Trg Dositeja Obradovića 3, 21000 Novi Sad, Serbia; branko.kordic@dh.uns.ac.rs (B.B.K.); milica.bogdanovic@dh.uns.ac.rs (M.G.B.); berta.hollo@dh.uns.ac.rs (B.B.H.); mirjana.lalovic@dh.uns.ac.rs (M.M.R.); dusan.skoric@dh.uns.ac.rs (D.Đ.Š.); branislav.jovic@dh.uns.ac.rs (B.D.J.)

[2] School of Chemical and Physical Sciences, Keele University, Keele ST5 5BG, UK; c.s.hawes@keele.ac.uk

* Correspondence: nikola.radnovic@dh.uns.ac.rs (N.D.R.); marko.rodic@dh.uns.ac.rs (M.V.R.)

Abstract: In this study, the synthesis of a Schiff base containing metal–organic frameworks (MOFs) of the UiO-67 family has been investigated. MOFs featuring free amine groups were successfully synthesized under mild solvothermal conditions using 2-amino-[1,1′-biphenyl]-4,4′-dicarboxylic acid and 2,2′-diamino-[1,1′-biphenyl]-4,4′-dicarboxylic acid as bridging ligands, resulting in MOFs with amine groups covalently linked to the bridging ligands. Both types of functionalized MOFs were post-synthetically modified with 4-formylbenzonitrile that resulted in imine formation. All the obtained compounds were characterized by PXRD, TGA, DTA, BET, NMR, and FTIR spectroscopy, while stability in water was monitored with SEM, EDS, and UV–VIS spectroscopy.

Keywords: coordination polymer; zirconium (IV); Schiff base; slow-release kinetics

Citation: Radnović, N.D.; Hawes, C.S.; Kordić, B.B.; Bogdanović, M.G.; Barta Holló, B.; Radanović, M.M.; Škorić, D.Đ.; Jović, B.D.; Rodić, M.V. Synthesis, Characterization, and Impact of Water on the Stability of Postmodified Schiff Base Containing Metal–Organic Frameworks. *Inorganics* **2023**, *11*, 432. https://doi.org/10.3390/inorganics11110432

Academic Editor: Isabel Correia

Received: 25 September 2023
Revised: 27 October 2023
Accepted: 3 November 2023
Published: 8 November 2023

1. Introduction

Metal–organic frameworks (MOFs) are organic–inorganic hybrid crystalline materials of high porosity. They consist of metal clusters connected by organic ligands (linkers). Among these, zirconium-based MOFs are the most promising due to their versatility in structural features and their stability and potential applications in different fields, such as gas adsorption, sensing, catalysis, drug delivery, etc. [1,2].

MOFs are promising efficient carbon-capture materials, as they are capable of selective adsorption of CO_2 from mixtures containing other gases, and their penalty for regeneration is minimal, particularly when pressure-swing desorption can be used [3,4]. One of the open challenges is their water sensitivity, which either competes with carbon dioxide or degrades MOF chemically [5]. As flue gas contains a large amount of water and pre-drying these gas streams is a costly engineering step, MOFs that can resist poisoning from water vapor are urgently needed [6].

To enhance the chemical stability of MOFs towards water, several approaches have been proposed [7–11], but the most effective one is the incorporation of high-oxidation-state metals and hydrophobic groups through their steric hindrance and repelling water [12]. Wang et al. [12] synthesized the zirconium MOF with 3,3′-bis(trifluoromethyl)-[1,1′-biphenyl]-4,4′-dicarboxylic acid (UiO-67-o-2CF_3) with great chemical stability due to the shielding effect of the trifluoromethyl groups. On the other hand, the same research group demonstrates that water stability can be achieved with hydrophilic groups such as the amino group, but only in the ortho-position of [1,1′-biphenyl]-4,4′-dicarboxylic acid due to intramolecular hydrogen bonding [13]. The advantage of using dicarboxylic ligands with amino groups as constituents of MOFs is their affinity for acidic CO_2.

The aim of this research was to find an easier synthetic approach that would achieve the same effect of water stability using more readily available building blocks for MOFs.

One of the useful approaches to adjusting the structure and the properties of MOFs to obtain better performance in the chosen field of use is post-synthetic modification. The research of the past decade suggests three major classes of these reactions, i.e., the post-synthetic ligand exchange, the post-synthetic metal exchange, and the post-synthetic elimination and insertion [14]. The idea of our research was to use the latter to protect the amino groups of the ligand via a reaction with a carbonyl compound which results in the formation of a Schiff base.

Their ease of synthesis, good yields, interesting coordination properties, and wide range of possible applications has led to Schiff bases being the focus of research of many coordination chemists for a long time [15,16]. The condensation of the free NH_2 group of the MOF with aromatic aldehydes should theoretically increase the steric hindrance, reducing the chance of water damaging the structure of the framework. In MOFs modified in this manner, the water would only cause damage to the imine group of the Schiff base and hydrolysis would occur, but the main framework would be preserved.

The synthesis of novel derivatives of UiO-67, i.e., UiO-67-NH_2 (**1**) and UiO-67-$(NH_2)_2$ (**2**), as well as their Schiff bases with 4-formylbenzonitrile (**1a**) and (**2a**) using postmodification approach, is presented. The obtained compounds were characterized using FT-IR, NMR, and XRD. The surface area of these compounds was analyzed via BET isotherm, and their bulk morphology was probed using SEM. The adsorption capacity and affinity towards CO_2 of the compounds were also determined. The stability of these Schiff bases in a water environment was monitored via UV–Vis spectroscopy.

2. Results and Discussion

2.1. Synthesis of the Compounds

The synthesis of 2-amino-[1,1′-biphenyl]-4,4′-dicarboxylic acid ($\mathbf{L^1}$) and 2,2′-diamino-[1,1′-biphenyl]-4,4′-dicarboxylic acid ($\mathbf{L^2}$) ligands was achieved in three-step synthetic pathways starting from the dimethyl ester of [1,1′-biphenyl]-4,4′-dicarboxylic acid (**I**), which entail nitration, reduction, and deprotection of the carboxylic acid, as shown in Schemes S1 and S2. The synthetic methodology is based on literature procedures [17–19] with minor modifications. Both the structures and purity of the ligands were confirmed by ^{1}H NMR (Figures S1 and S2) and FTIR spectra (Figures S3 and S4) which were in good agreement with the previously mentioned literature.

For the preparation of Schiff base-functionalized UiO-67 MOFs, the post-synthetic method was used. First, functionalized UiO-67 MOFs with one amine (**1**) and two amine groups (**2**) with $\mathbf{L^1}$ and $\mathbf{L^2}$ ligands were synthesized via the solvothermal reaction of $ZrCl_4$ and acetic acid as the modulator in DMF solution at 100 °C for 24 h in closed glass vials (Scheme 1).

The obtained MOFs, **1** and **2**, were used for Schiff base condensation with 4-formylbenzonitrile by soaking them in the MeOH solution of the aromatic aldehyde at room temperature for 24 h. This condensation (Scheme 2) resulted in two Schiff base-tagged UiO-67 MOFs: **1a** and **2a**.

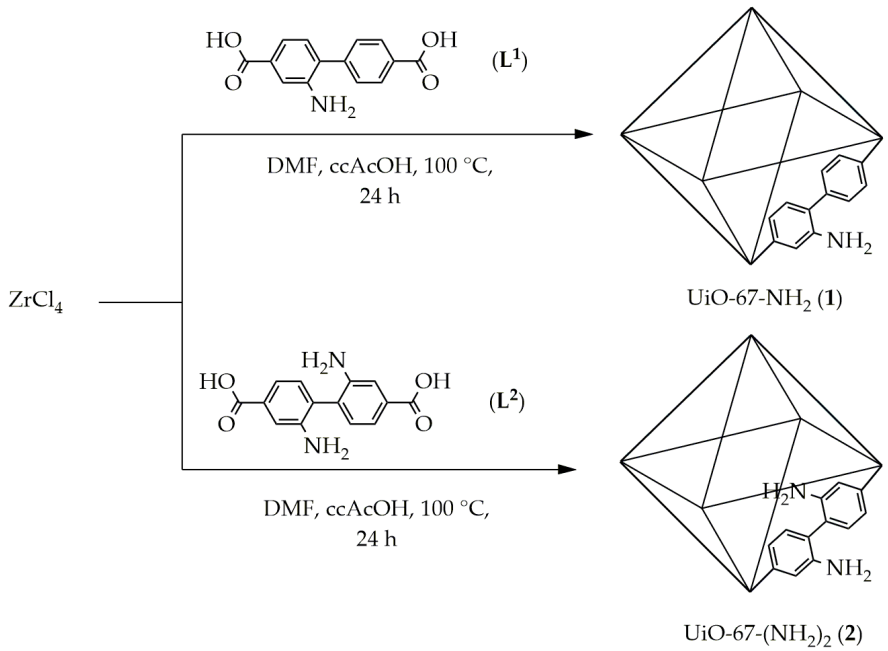

Scheme 1. Synthesis of **1** and **2**.

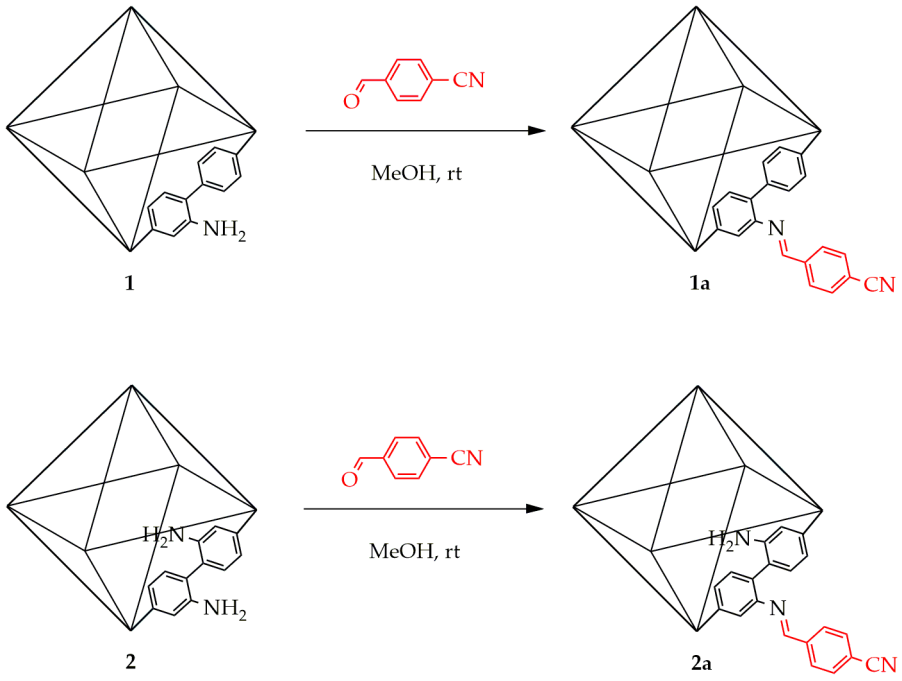

Scheme 2. Synthetic pathway to **1a** and **2a** from MOFs **1** and **2** via postmodification with 4-formylbenzonitrile.

2.2. Spectroscopic and Diffraction Characterization of the Compounds

Imine formation was evidenced by the FT-IR spectra of the isolated solids (Figure 1). After the final exchange with MeOH, the aldehyde ν(C=O) band at 1698 cm^{-1} was not observed, while the noticeable ν(C≡N) bands at 2231 cm^{-1} in **1** and 2232 cm^{-1} in **2** persisted, indicating the successful condensation without excess of unreacted aldehyde in the pores of MOFs.

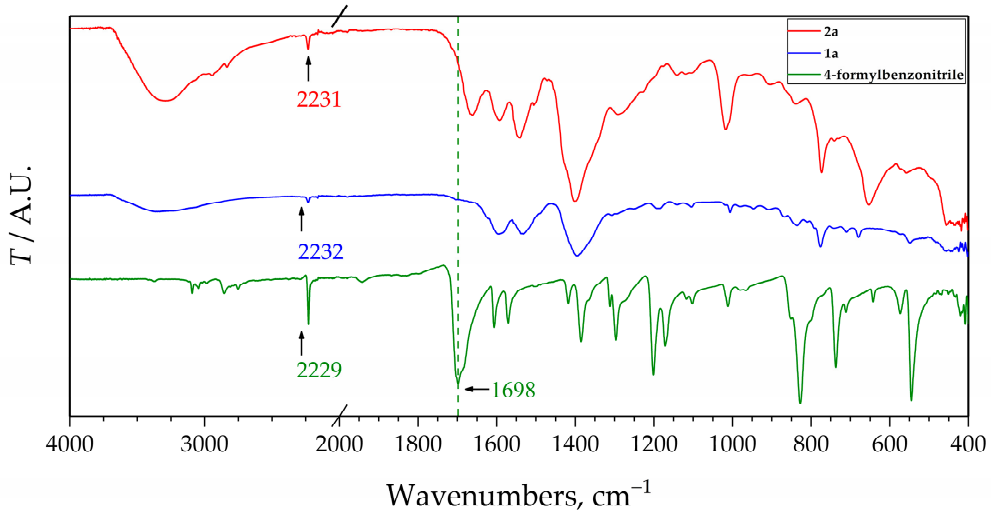

Figure 1. FT-IR spectra of **1a**, **2a**, and 4-formylbenzonitrile for comparison.

The powder X-ray diffraction (PXRD) patterns of **1a** and **2a** indicate that they share a structural similarity with UiO-67-NH2 (Figure 2), affirming that the incorporation of 4-formylbenzonitrile did not alter the fundamental structure of the MOFs. However, it is important to note that the formation of imines, while present, did not introduce any additional structural ordering within the MOFs. Consequently, the diffraction patterns alone do not provide conclusive confirmation of imine formation.

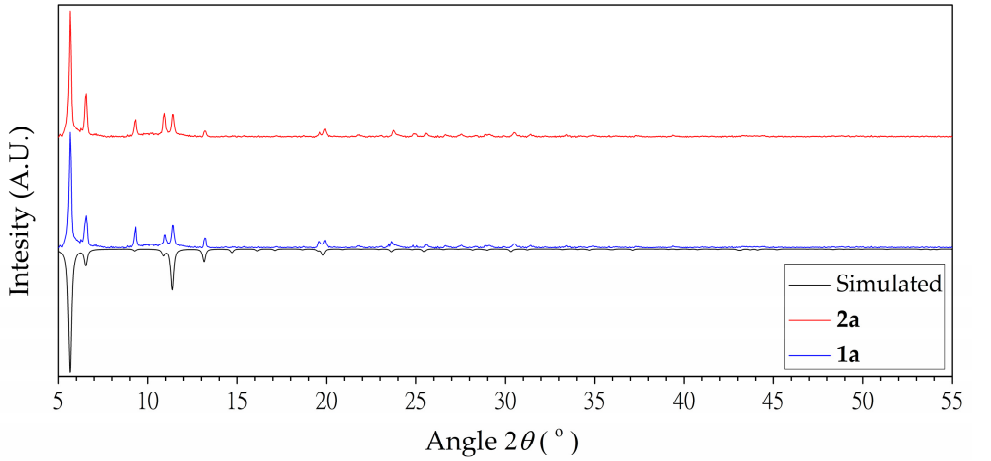

Figure 2. Comparison of room temperature X-ray powder diffraction data for **1a** and **2a** and pattern simulated from single crystal structure of UiO-67-NH_2 (CSD refcode JUSGOV, data at 150 K, [20]).

After digestion of MOFs in a trifluoroacetic acid-*d*/dimethyl sulfoxide-d_6 mixture, ^{1}H NMR data (Figure 3) show that the resulting solution contained both the Schiff base (sharp singlets at 8.85 ppm for **1a** and 8.72 ppm for **2a**), and products of its hydrolysis—the ligands $\mathbf{L^1}$ and $\mathbf{L^2}$ (sharp singlets at 8.28 ppm for **1a** and 7.65 ppm for **2a**) and 4-formylbenzonitrile (sharp singlets at 10.11 ppm in **1a** and 10.10 ppm in **2a**). Analyzing and integrating the intensities of clearly recognizable peaks and considering their ratio leads us to the conclusion that the percentage of condensed ligands and the success of postmodification can represent the ratio of the condensed and total ligand content. In case **1a**, the success rate was 80%, and in **2a** it was 46%. Based on the previous data, the successful postmodification of both MOFs was confirmed.

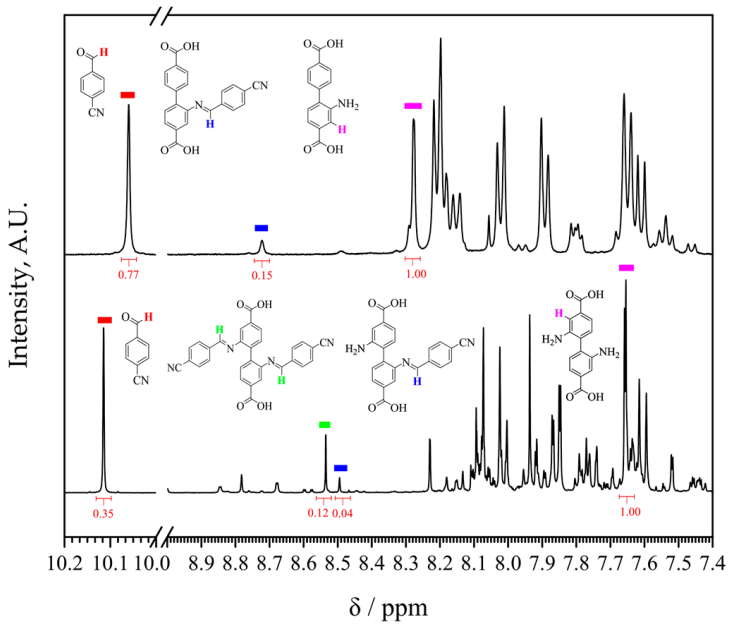

Figure 3. ^{1}H NMR of digested **1a** and **2a** in TFA/ DMSO-d_6.

2.3. Thermal Properties of the Compounds

The thermal stabilities of the prepared MOFs were studied via TGA experiments. The MOFs **1a** and **2a** were analyzed in argon. Both compounds began to lose mass at room temperature. Mass loss at a temperature this low is usually a consequence of evaporation of the absorbed solvent or environmental moisture. Compound **1a** lost 8.2% of its initial mass (m_0) up to 135 °C with a DTG maximum at 56 °C. The mass decrease above ~100 °C continued at a steadier rate and up to ~400 °C its amount was 5.4% of m_0. Above this temperature, the decomposition sped up and a well-defined mass loss of 28.6% was detected with a DTG maximum at 544 °C. This step may be correlated with the destruction of the MOF frameworks [21,22]. The thermal decomposition of the compound did not finish before reaching 700 °C (Figure 4).

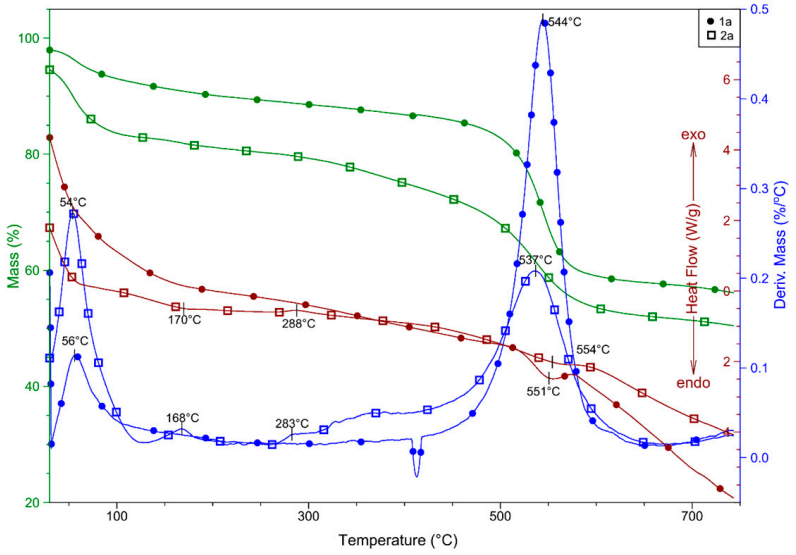

Figure 4. TG (green), DTG (blue), and DSC curves (brown) of compounds **1a** and **2a** in argon.

The freshly filtered compound **2a** lost 17.1% of m_0 up to 128 °C, and an additional 2.7% up to 260 °C. The corresponding DTG maxima were identified at 54 and 168 °C. The

thermal decomposition of **2a** continued with several highly overlapped processes and a total mass loss of 28.3%. The most intensive DTG maximum appeared at 537 °C. Above 600 °C, the decomposition of the compound slowed down, but it did not finish before reaching 700 °C.

Besides the desolvation, the thermal decomposition processes of **1a** and **2a** were followed by endothermic heat effects. In the case of **2a**, one exception was observed: a slight exothermic peak at 288 °C.

The evaporated solvent was analyzed with online coupled TG-MS measurements. Compound **1a** was losing methanol and water at room temperature, which was proven by the detected fragments m/z = 31 and 29 for methanol and m/z = 18 and 17 for water (Figure S6). The relative intensity of signals m/z = 17 and 18 was higher than that of m/z = 29 and 31. Similarly, compound **2a** was also losing water and methanol (Figure S7). During its analysis, the same fragments were detected as in the case of **1a**. Since the precursors were hydrated, traces of water were present in the reaction mixtures during syntheses of **1a** and **2a**. Thus, it was not surprising that products with absorbed water were obtained. On the other hand, water molecules are less voluminous and more polar than methanol molecules and may better fit into the pores of the MOFs and more easily form H-bonds.

2.4. Gas Adsorption

The surface characteristics of **1a** and **2a** were investigated using an N_2 sorption experiment. Based on the results obtained from sorption isotherms (Figure S8), the BET surface area for **1a** is 2091 m^2/g, the pore size is 12.7 Å, and the pore volume is 0.892 cm^3/g, while for **2a** the surface area is 1381 m^2/g, the pore size is 8.2 Å, and the pore volume is 0.623 tcm^3/g (Table S1). The second amino group on the bridging ligand in **2a** had an impact on the pore size and volume, making them smaller compared to pores in **1a**. Further, micropore size and volume influenced the overall surface area of MOFs, making the BET surface area of **2a** significantly lower than in the case of postmodified **1a**.

The obtained results are in accordance with the previously reported data. Wang et al. [13] obtained a value of UiO-67-m-$(NH_2)_2$ BET surface of 1196 m^2/g, while Ko et al. [23] reported a BET surface of 1360 and an average pore volume of 0.64 cm^3/g for the same MOF.

To determine the uptake of CO_2, a gas sorption experiment was carried out at 283, 288, and 293 K (Figure S9). The experiment showed that at the temperature of 293K and the pressure of 1 atm, **1a** has a maximum uptake of 67.1 cm^3(STP)/g, while **2a** has a maximum uptake of 58.2 cm^3(STP)/g. The obtained isosteric enthalpies of adsorption were similar for both MOFs: −38.6 kJ/mol for **1a** and −39.0 kJ/mol for **2a** (Figure S11). An adsorption enthalpy of −25.5 kJ/mol was reported for UiO-67-$(NH_2)_2$ [23], indicating a significantly stronger interaction between the adsorbent and adsorbate due to the postmodification.

2.5. Water Exposure Experiment

The process of hydrolysis, shown in Scheme 3, was investigated with the use of UV-VIS, FT-IR, and NMR spectroscopy. A change in the intensity of the band of 4-formyl benzonitrile at 252 nm was followed up. From Figure S12, it can be observed that the intensity of the band originating from the aldehyde increased with time, which indicates its gradual release. Additionally, there was no presence of ligand or Schiff base according to the absorption spectra, suggesting that there was no leak of structural constituents. The plateau was reached after around 6h, which can be seen on the graph of the relative released amounts of 4-formylbenzonitrile in water samples against time (Figure 5).

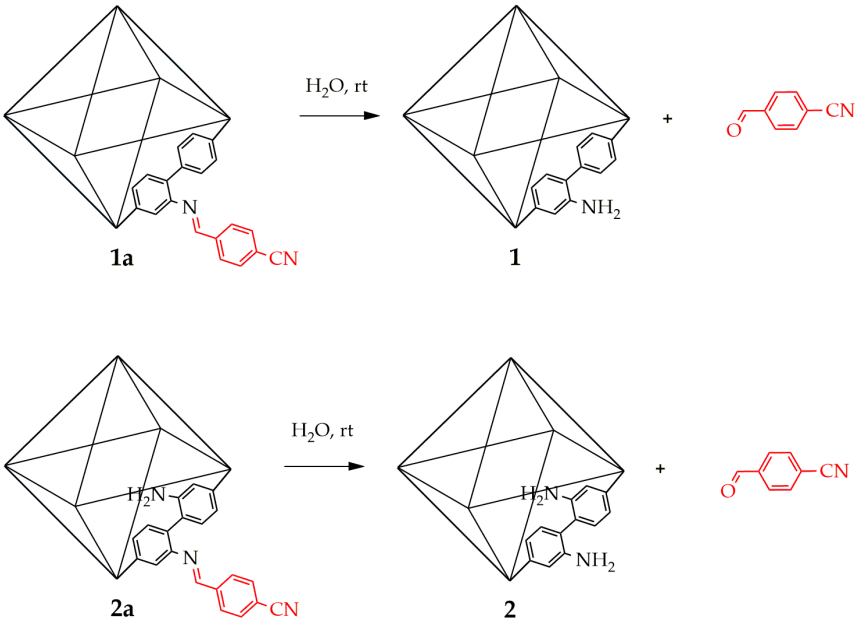

Scheme 3. Hydrolysis of postmodified **1a** and **2a.**

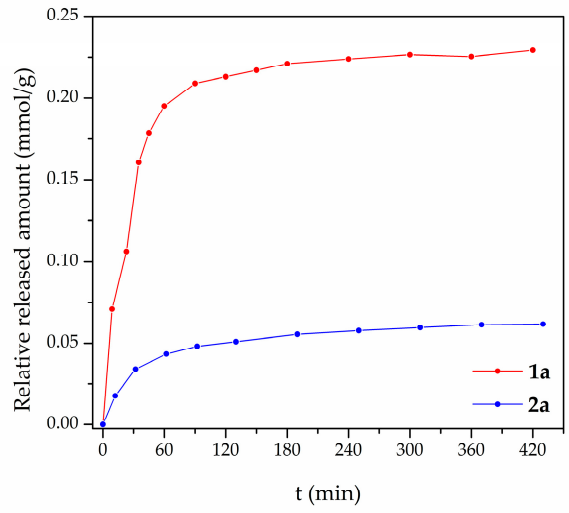

Figure 5. Relative released amounts of 4-formylbenzonitrile in water samples against time.

After previous water exposure, MOFs were digested in a trifluoroacetic acid-*d*/dimethyl sulfoxide-d_6 mixture and the ^{1}H NMR data obtained from it were compared with untreated specimens (Figure 6). From the relative ratios of peak intensities related to free ligand, 4-formylbenzonitrile, and Schiff base, drops in the percentages of postmodified ligand from 80% to 20% for **1a** and from 46% to 33% for **2a** were observed, which is in accordance with the relative released amount analyzed from the UV-VIS spectra.

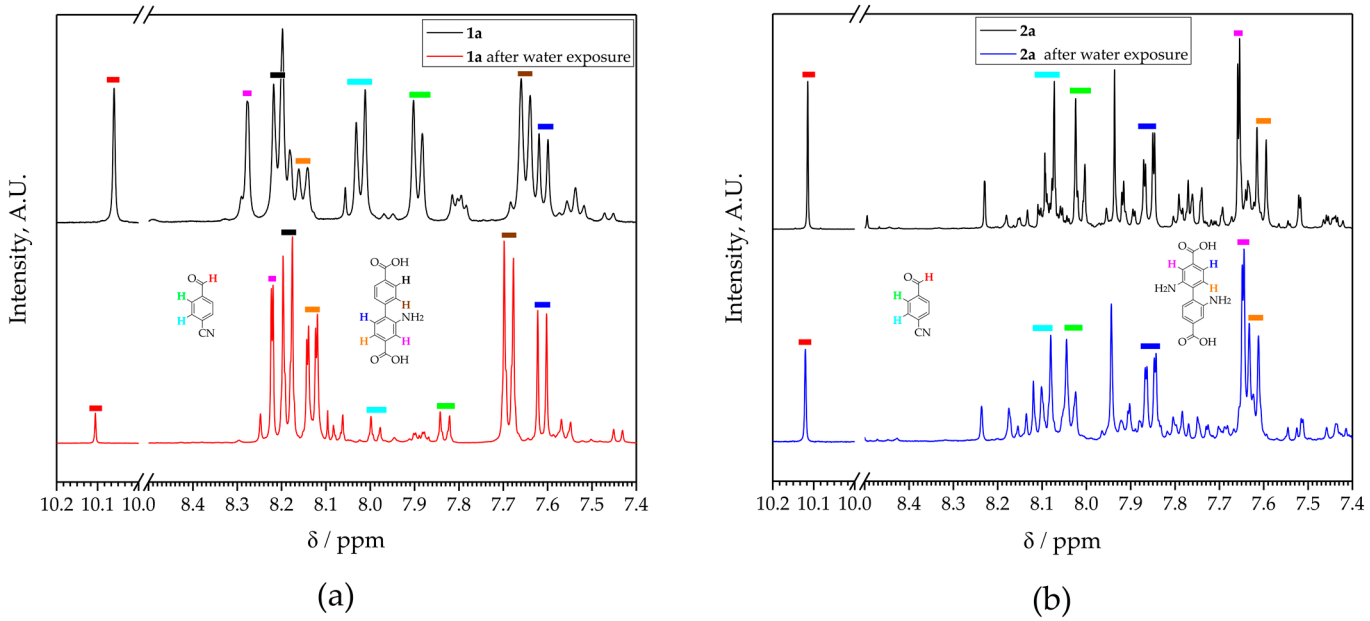

Figure 6. ^{1}H NMR spectra of digested **1a** (**a**) and **2a** (**b**) in TFA/DMSO-d_6 before (**top**) and after water exposure (**bottom**). Signals are marked with different colors where each of them represents proton with the same color in the structural formula.

The FT-IR spectra of MOFs collected after hydrolysis (Figure 7) also confirmed the release of aldehyde during water exposure, as reflected in the decrease in relative intensities of the ν(C≡N) vibrational band at 2232 cm^{-1} for **1a** and 2231 cm^{-1} for **2a**.

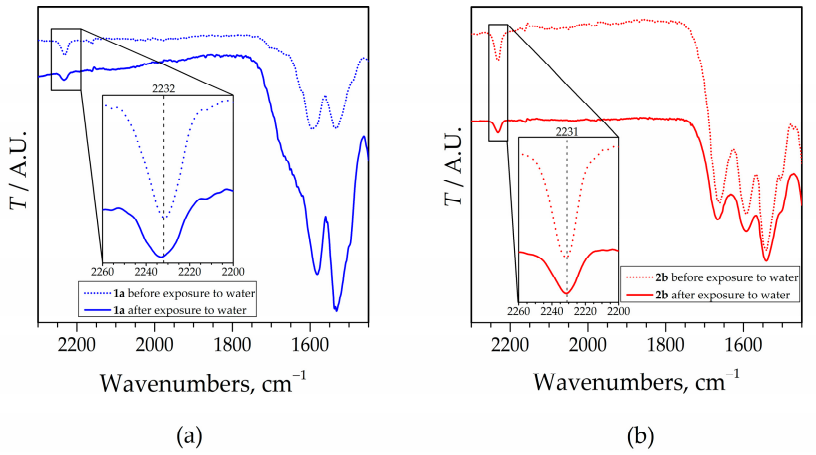

Figure 7. FT-IR spectra of **1a** (**a**) and **2a** (**b**) before and after water exposure during hydrolysis experiment.

2.6. Morphology of the Compounds

For the morphological study and stability of the crystallite surface of postmodified UiO-67 MOFs, SEM images were recorded. Figure 8 shows the morphological characteristics of the surface of the MOFs before (Figure 8a,b) and after hydrolysis (Figure 8c,d), from which it can be observed that the crystallite surface remained unchanged. In addition to the SEM analysis of the samples, energy-dispersive spectroscopy (EDS) was also performed, which identified certain elements present on the surface of the MOF crystals. Figure S13 shows the results of the EDS analysis, which corresponds well to the elemental composition of UiO-67 MOFs.

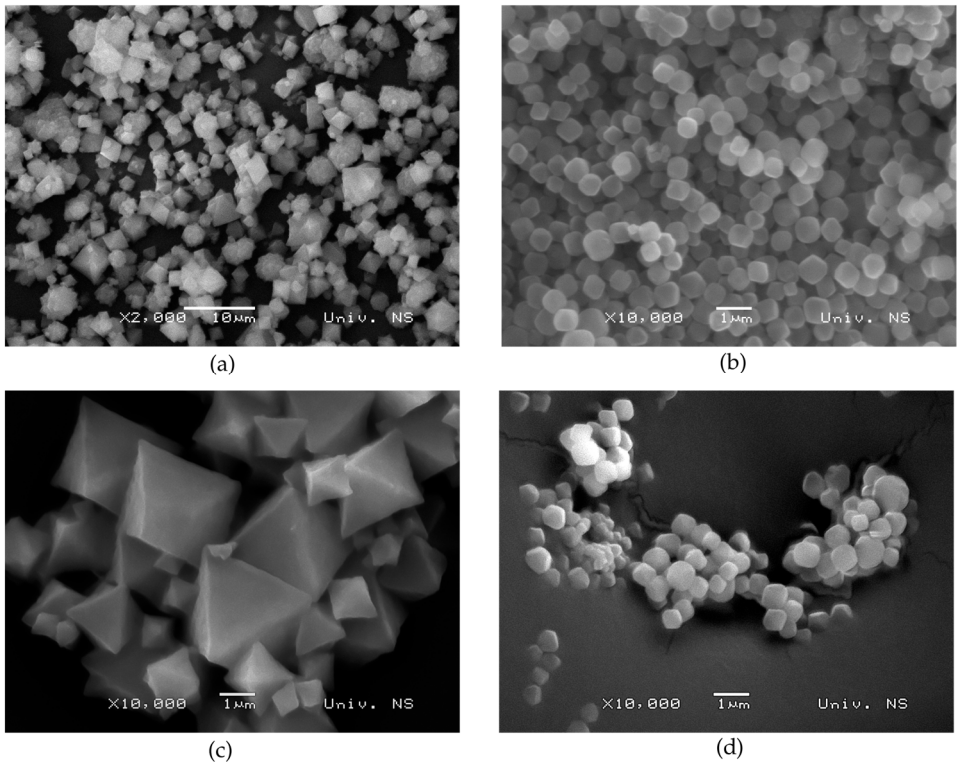

Figure 8. SEM images of **1a** and **2a** before (**a**,**b**) and after water treatment (**c**,**d**).

SEM micrographs (Figure S14) show that the crystal size of the MOFs ranged approximately from 1.30 µm to 2.70 µm for **1a** and from 490 nm to 800 nm for **2a**. The shape of **1a** before and after hydrolysis was octahedral and the shape of **2a** was approximately spherical; that is, all three dimensions were approximately equal. By increasing the resolution of the SEM micrograph, only the homogeneous and flat surface of the crystals could be observed. Magnification of up to 200,000 times showed no pores, which corresponds to MOFs which are well known for their microporosity. Also, the crystallinity of the sample after water treatment was demonstrated via X-ray powder diffraction (Figure S15), where both diffractograms match the pattern simulated from the crystal structure of UiO-67-NH_2.

3. Materials and Methods

3.1. Materials and Physical Measurements

All starting materials, reagents, and solvents purchased from Sigma-Aldrich (St Louis, MI, USA), Fluorochem (Glossop, UK), and Alfa Aesar (Haverhill, MI, USA) were of reagent grade or better, and were used as received. NMR spectroscopy was performed on a Bruker Avance III HD 400 spectrometer operating at 400 MHz for ^{1}H using deuterated solvents from Cambridge Isotope Laboratories. All spectra were referenced to the residual solvent signals. Infrared spectra were measured using a Thermo Scientific Nicolet iS10 instrument equipped with an ATR sampling accessory on a diamond crystal. UV-VIS spectra were collected on a Shimadzu UV-1800 UV/Visible Scanning Spectrophotometer, using 1 cm UVIRSIL cells. X-ray powder diffraction patterns were measured on a Bruker D8 Advance diffractometer with a Cu-Kα source (λ = 1.54178 Å). Samples were mounted on a zero-background silicon single-crystal sample holder. All samples were measured at room temperature in the 2θ range 5–55°.

The simultaneous thermogravimetric–differential scanning calorimetric measurements (TG–DSC) were carried out on a TA Instruments SDT Q600 thermal analyzer from room temperature up to 700 °C in an argon atmosphere and flow rate 50 cm^3 min^{-1}. The heating rate was 10 °C min^{-1}. The sample (1–2 mg) was placed in an alumina crucible, and an empty alumina crucible was the reference. The analysis of the evolved gaseous products

was carried out on a Hiden Analytical HPR20/QIC mass spectrometer coupled to the SDT Q600 thermal analyzer. The selected fragments in the range $15 < m/z < 80$ were followed in Multiple Ion Detection (MID) modes.

Gas adsorption measurements were performed using a Quantachrome Autosorb iQ using N_2 and CO_2 at N4.5 grade or better. Temperature control was provided by a liquid nitrogen dewar for N_2 measurements and a Julabo recirculating chiller for CO_2 measurements. Samples were activated prior to the adsorption experiment by soaking in methanol for 3 days, exchanging for fresh solvent every 12 h. Initial activation was performed at 100 °C under a dynamic vacuum provided by a rotary oil pump followed by soaking under a high vacuum provided by a turbomolecular pump at 100 °C for 12 h.

SEM images and EDS spectra were collected on a JEOL JSM 6460 LV scanning electron microscope with an Oxford INCA EDS device. Samples were vaporized with a layer of gold in a high vacuum in a BAL-TEC, SCD 005 SPUTTER COATER for the preparation of samples by gold sputtering under a high vacuum (30mA WD 10mm) for 90 s.

3.2. Preparation of the Compounds

3.2.1. Synthesis of 2-amino-4,4′-biphenyldicarboxylic Acid ($\mathbf{L^1}$) and 2,2′-diamino-4,4′-biphenyldicarboxylic Acid ($\mathbf{L^2}$)

Ligands $\mathbf{L^1}$ and $\mathbf{L^2}$ were synthesized according to the procedures reported in the literature [17–19] with some modifications, details of which are given in the Supplementary Materials.

3.2.2. Synthesis of UiO-67-NH_2 (**1**) and UiO-67-$(NH_2)_2$ (**2**)

2-amino-4,4′-biphenyldicarboxylic acid (38.6 mg, 0.15 mmol, 1.0 eq.)/2,2′-diamino-4,4′-biphenyldicarboxylic acid (40.84 mg, 0.15 mmol, 1.0 eq.) and glacial acetic acid (0.35 mL) were added to DMF (3 mL). This solution was added to $ZrCl_4$ (36 mg, 0.15 mmol, 1.0 eq.) in DMF (3 mL) and sonicated for 5 min. The vial was then sealed and heated overnight at 100 °C. The resulting mixture was allowed to cool, and the resulting precipitate was collected by filtration and washed with DMF (3 × 1 mL) and then MeOH (1 mL) to yield a fine, pale-yellow solid (**1**)/a fine yellow solid (**2**). For FT-IR and NMR measurements, to eliminate the influence of DMF, the material was immersed in MeOH for 15 min with the solvent being exchanged with fresh MeOH (3 mL) every 2 min.

ν_{max}/cm^{-1} (ATR) for **1**: 3333 w, 2943 w, 2832 w, 1586 m, 1541 m, 1405 s, 1279 w, 1245 w, 1183 w, 1147 w, 1105 w, 1019 s, 870 w, 772 s, 712 m, 653 s, 433 s, 406 s.

ν_{max}/cm^{-1} (ATR) for **2**: 3249 w, 1667 w, 1592 w, 1538 m, 1402 s, 1273 w, 1139 w, 1004 w, 772 m, 674 s, 442 s, 430 s, 403 s.

3.2.3. Synthesis of **1a** and **2a**

UiO-67-NH_2 (44 mg, 0.02 mmol)/ UiO-67-$(NH_2)_2$ (46 mg, 0.02 mmol) was dispersed with 5 mL of MeOH in a vial. In the resulting suspension, 4-formylbenzonitrile (50 mg, 0.38 mmol) was added and the final mixture was left at room temperature. The resulting precipitate was immersed in fresh MeOH that was exchanged 5 times to eliminate the influence of unreacted benzaldehyde during FT-IR and NMR measurements.

ν_{max}/cm^{-1} (ATR) for **1a**: 3335 w, 2232 w, 1594 m, 1533 m, 1394 s, 1307 w, 1186 w, 1141 w, 1105 w, 1006 w, 947 w, 908 w, 836 m, 776 s, 742 m, 710 m, 679 m, 549 s, 445 s, 411 s, 402 s.

ν_{max}/cm^{-1} (ATR) for **2a**: 3292 w, 2231 w, 2945 w, 2834 w, 1662 m, 1593 m, 1541 m, 1402 s, 1292 m, 1141 w, 1017 m, 840 w, 773 s, 653 s, 557 s, 456 s, 437 s, 406 s.

3.3. Gas Adsorption of the Compounds

Immersion of the solids in MeOH for 3 days, refreshing the solvent every 12 h, effected complete exchange of the DMF guests within the pores, and post exchange both materials reached complete desolvation below 100 °C with TGA. The exchanged materials were

activated at 100 °C under dynamic vacuum overnight prior to nitrogen and carbon dioxide adsorption measurements.

3.4. Water Exposure of the Compounds

The experiment consisted of immersion of **1a** (11.7 mg) and **2a** (48.2 mg) in H_2O (400 mL) with slight stirring for 7 h and sampling and filtering the solution through a syringe filter for collecting the UV-VIS spectra in the range of 210 to 310 nm every 15 min. The spectrophotometer was calibrated with standard solutions of 4-formylbenzonitrile, and all absorbance measurements were performed at a wavelength of 252 nm. After monitoring the aldehyde release in water through absorbance, solids of **1a** and **2a** were filtered and dried in air for NMR, FT-IR, SEM and EDS analysis.

4. Conclusions

A Zr-based MOF UiO-67 was successfully synthesized via direct solvothermal methods and post-synthetically modified with 4-formylbenzonitrile to introduce imine functionality. Extensive analyses involving FTIR and ^{1}H NMR spectroscopy have unequivocally demonstrated that the aldehyde groups react with the amine groups of the ligand, rather than being simply encapsulated within the material's pores. Additional characterizations, including XRD analysis, thermogravimetry, and SEM imaging, have affirmed that the formation of a Schiff base does not disrupt the overall crystal structures and morphologies of the initial compounds.

The presence of a Schiff base affects the affinity of these MOFs towards CO_2, increasing the interaction between adsorbent and adsorbate, which is favorable for using these materials for carbon capture and environmental protection.

Upon exposure to water, the postmodified MOFs undergo hydrolysis, resulting in the gradual release of aldehyde, without any evidence of leakage of structural constituent. The NMR data acquired following hydrolysis indicate a significant reduction in the postmodified ligand content, from 80% to 20% for **1a** and from 46% to 33% for **2a**.

Although MOFs synthesized with 3,3′-bis(trifluoromethyl)-[1,1′-biphenyl]-4,4′-dicarboxylic acid (UiO-67-o-2CF_3) and 3,3′-diamino-[1,1′-biphenyl]-4,4′-dicarboxylic acid (UiO-67-o-2NH_2) exhibit excellent stability, their synthetic routes involve pricier reagents and additional steps compared to our method. Our approach offers the advantage of a simpler four-step synthesis, eliminating the need for time-consuming and costly reagents. A drawback of our approach is the intentional hydrolysis of the Schiff base in the postmodified ligand. However, this property can be harnessed for other applications, such as controlled drug release, opening up opportunities for further research in this direction.

These specific findings underscore the promising potential for future research focused on harnessing the controlled, slow release of reversibly covalently grafted molecules from amine-containing MOFs.

Supplementary Materials: The following supporting information can be downloaded at: https://www.mdpi.com/article/10.3390/inorganics11110432/s1, Scheme S1. Synthesis of $\mathbf{L^1}$. Reagents and conditions: (a) ccH_2SO_4, 65% HNO_3 (1 eq.), 15 °C, 2 h; (b) Pd/C, MeOH, THF, 60 °C, 2 h (c) 1 M KOH, THF/H_2O, reflux, 16 h, then 1M HCl; Scheme S2. Synthesis of $\mathbf{L^2}$. Reagents and conditions: (a) cc H_2SO_4, 65% HNO_3 (2 eq.), 15–20 °C, 2 h; (b) Pd/C, MeOH, THF, 60 °C, 2 h (c) 2M KOH, THF/H_2O, reflux, 16 h, then 2M HCl; Figure S1. The ^{1}H NMR spectrum (400MHz, DMSO-d_6) of $\mathbf{L^1}$; Figure S2. The ^{1}H NMR spectrum (400 MHz, DMSO-d_6) of $\mathbf{L^2}$; Figure S3. FT-IR Spectra of ligand ($\mathbf{L^1}$) and intermediates (**IIa** and **IIIa**) of three-step synthetic pathway for comparison; Figure S4. FT-IR Spectra of ligand ($\mathbf{L^2}$) and intermediates (**Iib** and **IIIb**) of three-step synthetic pathway for comparison; Figure S5. FT-IR spectra of **1**, **2**, and corresponding ligands for comparison; Figure S6. TG–MS signals of fragments evolved from **1a** during heating in argon; Figure S7. TG–MS signals of fragments evolved from **2a** during heating in argon; Figure S8. N_2 sorption isotherms for (a) **1a** and (b) **2b;** Figure S9. CO_2 sorption isotherms for (a) **1a** and (b) **2a** at 283, 288, and 293 K; Figure S10. Virial fit of CO_2 adsorption data for (a) **1a** and (b) **2a** at 283, 288, and 293 K; Figure S11. Isosteric enthalpy of adsorption obtained from virial fit for (a) **1a** and (b) **2a**; Table S1. Gas sorption investigation data;

Table S2. Obtained virial parameters; Figure S12. UV spectra of water samples containing (a) **1a** and (b) **2a** collected at different time intervals; Figure S13. Selected surfaces of **1a** (a) and **2a** (b) for EDS analysis and their spectra (c,d); Figure S14. SEM micrographs of 1a (a) and 2a (b) that show the variety of crystal sizes; Figure S15. X-ray powder diffraction data for **1a** and **2a** after exposure to water.

Author Contributions: Conceptualization, N.D.R., M.V.R., B.B.K. and B.B.H.; investigation, N.D.R., B.B.K., C.S.H., M.G.B., M.V.R. and B.B.H.; resources, C.S.H., N.D.R. and B.B.H.; writing—original draft preparation, N.D.R., B.B.H., B.B.K., M.M.R. and M.V.R.; writing—review and editing, B.B.H., M.V.R., C.S.H., B.D.J. and M.M.R.; visualization, N.D.R., B.B.K., D.Đ.Š. and B.B.H.; supervision, B.D.J., M.V.R. and M.M.R.; project administration, M.V.R. and M.M.R.; funding acquisition, B.B.H., M.V.R. and M.M.R. All authors have read and agreed to the published version of the manuscript.

Funding: This research was funded by the Science Fund of the Republic of Serbia, PROMIS grant number 6066708 (CASCH-MOF), the Ministry of Science, Technological Development and Innovation of the Republic of Serbia (Grant No. 451-03-47/2023-01/200125) and the Provincial Secretariat for Higher Education and Scientific Research (Grant No. 42-451-2197/2022).

Data Availability Statement: The data presented in this study are available in supplementary materials.

Acknowledgments: The authors gratefully acknowledge Marko Radenković and Miloš Bokorov from Department of Biology and Ecology, Faculty of Sciences, University of Novi Sad for their invaluable assistance with capturing images using the secondary electron microscope, which greatly enhanced the visual representation of our research in this article. We are grateful to Dr Jelena Tričković for her initial involvement in the project and fruitful discussions.

Conflicts of Interest: The authors declare no conflict of interest.

References

1. Jia, C.; He, T.; Wang, G.M. Zirconium-Based Metal-Organic Frameworks for Fluorescent Sensing. *Coord. Chem. Rev.* **2023**, *476*, 214930. [CrossRef]
2. Ji, Q.; Zou, L.; Liu, H.; Yong, J.; Chen, J.; Song, Z.; Gao, J. Bimetallic Nanoparticles Embedded in N-Doped Carbon Nanotubes Derived from Metal-Organic Frameworks as Efficient Electrocatalysts for Oxygen Evolution Reaction. *J. Solid State Chem.* **2021**, *303*, 122515. [CrossRef]
3. Lin, J.-B.; Nguyen, T.T.T.; Vaidhyanathan, R.; Burner, J.; Taylor, J.M.; Durekova, H.; Akhtar, F.; Mah, R.K.; Ghaffari-Nik, O.; Marx, S.; et al. A Scalable Metal-Organic Framework as a Durable Physisorbent for Carbon Dioxide Capture. *Science* **2021**, *374*, 1464–1469. [CrossRef] [PubMed]
4. Sumida, K.; Rogow, D.L.; Mason, J.A.; McDonald, T.M.; Bloch, E.D.; Herm, Z.R.; Bae, T.-H.; Long, J.R. Carbon Dioxide Capture in Metal–Organic Frameworks. *Chem. Rev.* **2012**, *112*, 724–781. [CrossRef]
5. Burtch, N.C.; Jasuja, H.; Walton, K.S. Water Stability and Adsorption in Metal–Organic Frameworks. *Chem. Rev.* **2014**, *114*, 10575–10612. [CrossRef]
6. Madden, D.G.; Scott, H.S.; Kumar, A.; Chen, K.J.; Sanii, R.; Bajpai, A.; Lusi, M.; Curtin, T.; Perry, J.J.; Zaworotko, M.J. Flue-Gas and Direct-Air Capture of CO2 by Porous Metalorganic Materials. *Philos. Trans. R. Soc. A Math. Phys. Eng. Sci.* **2017**, *375*, 20160025. [CrossRef]
7. Li, N.; Xu, J.; Feng, R.; Hu, T.-L.; Bu, X.-H. Governing Metal–Organic Frameworks towards High Stability. *Chem. Commun.* **2016**, *52*, 8501–8513. [CrossRef]
8. Xie, X.-Y.; Qian, X.-Y.; Qi, S.-C.; Wu, J.-K.; Liu, X.-Q.; Sun, L.-B. Endowing Cu-BTC with Improved Hydrothermal Stability and Catalytic Activity: Hybridization with Natural Clay Attapulgite via Vapor-Induced Crystallization. *ACS Sustain. Chem. Eng.* **2018**, *6*, 13217–13225. [CrossRef]
9. Lu, L.; Li, X.-Y.; Liu, X.-Q.; Wang, Z.-M.; Sun, L.-B. Enhancing the Hydrostability and Catalytic Performance of Metal–Organic Frameworks by Hybridizing with Attapulgite, a Natural Clay. *J. Mater. Chem. A* **2015**, *3*, 6998–7005. [CrossRef]
10. Øien-Ødegaard, S.; Bouchevreau, B.; Hylland, K.; Wu, L.; Blom, R.; Grande, C.; Olsbye, U.; Tilset, M.; Lillerud, K.P. UiO-67-Type Metal–Organic Frameworks with Enhanced Water Stability and Methane Adsorption Capacity. *Inorg. Chem.* **2016**, *55*, 1986–1991. [CrossRef]
11. Ma, D.; Li, Y.; Li, Z. Tuning the Moisture Stability of Metal–Organic Frameworks by Incorporating Hydrophobic Functional Groups at Different Positions of Ligands. *Chem. Commun.* **2011**, *47*, 7377–7379. [CrossRef] [PubMed]
12. Wang, K.; Huang, H.; Zhou, X.; Wang, Q.; Li, G.; Shen, H.; She, Y.; Zhong, C. Highly Chemically Stable MOFs with Trifluoromethyl Groups: Effect of Position of Trifluoromethyl Groups on Chemical Stability. *Inorg. Chem.* **2019**, *58*, 5725–5732. [CrossRef] [PubMed]
13. Wang, K.; Wang, Q.; Wang, X.; Wang, M.; Wang, Q.; Shen, H.-M.; Yang, Y.-F.; She, Y. Intramolecular Hydrogen Bond-Induced High Chemical Stability of Metal–Organic Frameworks. *Inorg. Chem. Front.* **2020**, *7*, 3548–3554. [CrossRef]

14. Yin, Z.; Wan, S.; Yang, J.; Kurmoo, M.; Zeng, M.H. Recent Advances in Post-Synthetic Modification of Metal–Organic Frameworks: New Types and Tandem Reactions. *Coord. Chem. Rev.* **2019**, *378*, 500–512. [CrossRef]
15. Liu, X.; Manzur, C.; Novoa, N.; Celedón, S.; Carrillo, D.; Hamon, J.R. Multidentate Unsymmetrically-Substituted Schiff Bases and Their Metal Complexes: Synthesis, Functional Materials Properties, and Applications to Catalysis. *Coord. Chem. Rev.* **2018**, *357*, 144–172. [CrossRef]
16. Kumar, M.; Singh, A.K.; Singh, A.K.; Yadav, R.K.; Singh, S.; Singh, A.P.; Chauhan, A. Recent Advances in 3d-Block Metal Complexes with Bi, Tri, and Tetradentate Schiff Base Ligands Derived from Salicylaldehyde and Its Derivatives: Synthesis, Characterization and Applications. *Coord. Chem. Rev.* **2023**, *488*, 215176. [CrossRef]
17. Olkhovik, V.K.; Vasilevskii, D.A.; Pap, A.A.; Kalechyts, G.V.; Matveienko, Y.V.; Baran, A.G.; Halinouski, N.A.; Petushok, V.G. Synthesis of New Polyconjugated Molecules with Biphenyl, Dibenzothiophene, Carbazole and Phenanthrene Units. *Arkivoc* **2008**, *2008*, 69–93. [CrossRef]
18. Khansari, A.; Bryant, M.R.; Jenkinson, D.R.; Jameson, G.B.; Qazvini, O.T.; Liu, L.; Burrows, A.D.; Telfer, S.G.; Richardson, C. Interpenetration Isomers in Isoreticular Amine-Tagged Zinc MOFs. *CrystEngComm* **2019**, *21*, 7498–7506. [CrossRef]
19. Deshpande, R.K.; Minnaar, J.L.; Telfer, S.G. Thermolabile Groups in Metal–Organic Frameworks: Suppression of Network Interpenetration, Post-Synthetic Cavity Expansion, and Protection of Reactive Functional Groups. *Angew. Chem. Int. Ed.* **2010**, *49*, 4598–4602. [CrossRef]
20. Kaposi, M.; Cokoja, M.; Hutterer, C.H.; Hauser, S.A.; Kaposi, T.; Klappenberger, F.; Pöthig, A.; Barth, J.V.; Herrmann, W.A.; Kühn, F.E. Immobilisation of a Molecular Epoxidation Catalyst on UiO-66 and -67: The Effect of Pore Size on Catalyst Activity and Recycling. *Dalton Trans.* **2015**, *44*, 15976–15983. [CrossRef]
21. Mohammadi, L.; Khavasi, H.R. Anthracene-Tagged UiO-67-MOF as Highly Selective Aqueous Sensor for Nanoscale Detection of Arginine Amino Acid. *Inorg. Chem.* **2020**, *59*, 13091–13097. [CrossRef] [PubMed]
22. Pal, A.; Chand, S.; Das, M.C. A Water-Stable Twofold Interpenetrating Microporous MOF for Selective CO2 Adsorption and Separation. *Inorg. Chem.* **2017**, *56*, 13991–13997. [CrossRef] [PubMed]
23. Ko, N.; Hong, J.; Sung, S.; Cordova, K.E.; Park, H.J.; Yang, J.K.; Kim, J. A Significant Enhancement of Water Vapour Uptake at Low Pressure by Amine-Functionalization of UiO-67. *Dalton Trans.* **2015**, *44*, 2047–2051. [CrossRef] [PubMed]